Relative Rotor Phasing for Multicopter Vibratory Load Minimization

Robert Niemiec
Research Scientist

Farhan Gandhi
Redfern Professor and MOVE Director

Nicholas Kopyt
Undergraduate Research Assistant

Center for Mobility With Vertical Lift (MOVE)
Rensselaer Polytechnic Institute
Troy, NY, United States

ABSTRACT

This study focuses on vibration reduction for quadcopters and octocopters with elastic, 2-bladed, synchronized-RPM, variable-pitch rotors through the use of relative rotor phasing. The study defines phase modes such as a pitch phase mode with relative phasing between the front and aft rotors, a roll phase mode with relative phasing between the left and right rotors, and a differential phase mode with relative phasing between the clockwise and counterclockwise spinning rotors for both the quadcopter and the octocopter, as well as additional higher harmonic phase modes for the octocopter. Parametric studies on individual phase modes indicate that for the quadcopter in forward flight the pitch and roll phase modes can almost entirely eliminate the 2/rev vibratory forces (at the aircraft level), but the 2/rev vibratory moments cannot be minimized at the same time. By simultaneously using multiple phase modes a Pareto-front can be generated and a solution selected based on the relative emphasis on force or moment vibration reduction. For the octocopter it was observed that individual higher harmonic modes (specifically the 2c or 2s modes) could almost entirely eliminate both the 2/rev vibratory forces and moments, simultaneously. Compared to vibration levels in forward flight that might, on average, be expected if the rotors were randomly phased, reductions of 62% and 96% in a composite vibration index (equally weighting 2/rev vibratory forces and moments) were calculated for the quadcopter and octocopter, respectively, with appropriate rotor phasing.

NOTATION

F_2	- 2-norm force vibration index (N)
M_2	- 2-norm moment vibration index (Nm)
N_r	- number of rotors
Ω	- rotor speed (RPM)
Φ_R	- roll phasing (deg)
Φ_P	- pitch phasing (deg)
Φ_D	- differential phasing (deg)
Φ_{2s}	- 2s phasing (deg)
Φ_{2c}	- 2c phasing (deg)
Ψ_k	- azimuthal location of rotor k (deg)
ψ_k	- azimuthal position of rotor k blades (deg)
θ_k	- root pitch of rotor k (deg)
θ_0	- collective pitch control (deg)
θ_{1s}	- lateral pitch control (deg)
θ_{1c}	- longitudinal pitch control (deg)
θ_d	- differential pitch control (deg)

INTRODUCTION

While small multicopters have been in operation and in use by hobbyists and videographers for quite some time, there has been an enormous and rapidly growing recent interest in scaling-up to much larger electric multi-rotor aircraft (eVTOL aircraft) for military use, commercial use including package delivery, and even passenger transportation (Refs. 1–3). Development of these large eVTOL aircraft faces many challenges (Ref. 4), and has led to significant investigation and new understanding in areas such as multi-rotor interactional aerodynamics (Refs. 5–10), acoustics (Refs. 11–20), and handling qualities (Refs. 21–26). An area that has received much less attention so far, but is equally important to operation, comfort and cost, is the vibration characteristics of eVTOL aircraft. A study in (Ref. 27) highlighted a beating phenomenon observed with the vibratory loads of a quadcopter due to the rotors operating at different rotational speeds.

On account of their tremendous simplicity and associated cost benefits, fixed-pitch, variable-RPM rotors have generally been the rotors of choice on eVTOL configurations. However, the increase in rotor diameter (and rotational inertia) with increasing gross weight, can result in degradation in the eVTOL aircraft's handling qualities for reasonable motor size (Refs. 21–24), and this has led to an interest in variable collective pitch on the rotors for improved flying qualities (Refs. 25, 26). The presence of collective pitch control can also be beneficial for conditions such as climb (Ref. 28). Introduction of collective pitch control allows for RPM synchronization and relative phase control of the rotors, which can further be exploited for noise reduction (Refs. 18–20) and vibration reduction (Ref. 29).

Presented at the VFS International 76th Annual Forum & Technology Display, Virginia Beach, VA, October 6–8, 2020. Copyright © 2020 by the Vertical Flight Society. All rights reserved.

In Ref. 29, the authors consider relative rotor phase control on RPM-synchronized plus- and cross-configuration quadcopters with variable collective pitch, but the study made the simplifying assumption that the effects of elastic blade deformation were negligible. The present study seeks to expand the work of Ref. 29 by including the effect of elastic blade deformation on the vibratory loads, and examining the effect of relative rotor phasing on vibratory load reduction of both a quadcopter as well as an octocopter.

MODELLING AND VALIDATION

Simulations in this study are carried out using the Rensselaer Multicopter Analysis Code (RMAC, Ref. 30). RMAC has available both rigid-blade as well as an elastic blade modeling capabilities for the rotors. While the former is frequently utilized in flight simulation and handling qualities studies, (e.g., Refs. 21–24,26) elastic blade models are the appropriate choice for studies on vibratory loads. In Ref. (Ref. 29), blade elastic flap and lag deflections (but not torsion) were modeled, but RMAC was extended to include the fully coupled nonlinear elastic flap-lag-torsion equations based on Hodges and Dowell (Ref. 31) in the present study. The blades are spatially discretized using a Ritz modal representation with two modes each in flapwise bending, lagwise bending, and elastic torsion (bending and torsion modes shapes are shown in Fig. 1). The rotor aerodynamic loads are calculated using blade-element theory coupled to a 10-state Peters-He finite-state wake model (Ref. 32) to calculate the induced velocities. The blade periodic response is calculated using the harmonic balance method and integration of the blade loads over the span and the azimuth and summation over both blades (for the two-bladed rotors used in the present study) yields the rotor hub forces and moments.

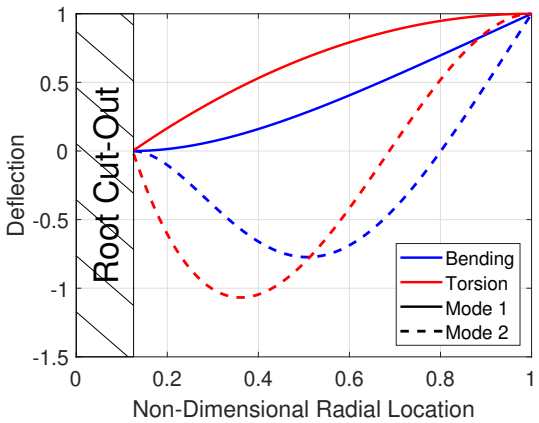

Figure 1: Elastic bending and torsion modes

The elastic blade model was validated against experimental results from Ref. 33. The rotor used in this study taken from the DJI Phantom, and made from ABS plastic. Geometric and elastic properties of this rotor are listed in Table 1. The blade chord and twist distributions for the DJI rotor are taken from Ref. 7, and the mass distribution is assumed to scale with the area of the cross-section (uniform density).

Table 1: Summary of DJI rotor parameters

DJI rotor parameters	
Rotor Radius	0.12 m
Young's Modulus	1.0 MPa
Shear Modulus	0.385 MPa
Poisson's Ratio	0.30
Blade Mass	12 g

The static thrust of the DJI rotor predicted by RMAC is compared to the experimental data in Fig. 2. RMAC shows good agreement in the low-to-moderate thrust range. While greater difference is observed at higher thrust, the maximum difference is under 16%.

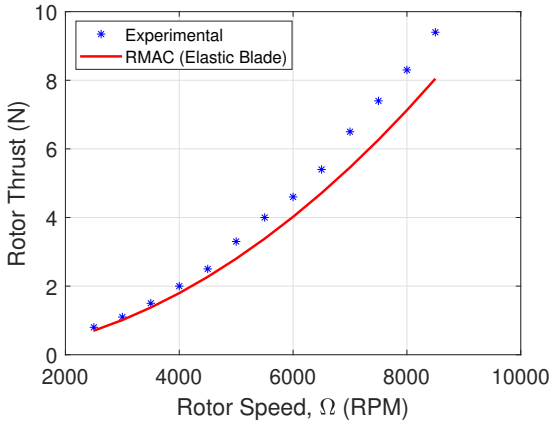

Figure 2: Predicted and experimental thrust – DJI rotor

The RMAC-predicted values of the out-of-plane deflection and torsion are compared to the measurements of Ref. 33 in Figs. 3 and 4. The trends of both flap and torsion are captured by the RMAC model, with increased RPM (and thrust) resulting in greater flapwise and nose-down torsional deflection, with particularly good agreement in the flapwise deflection.

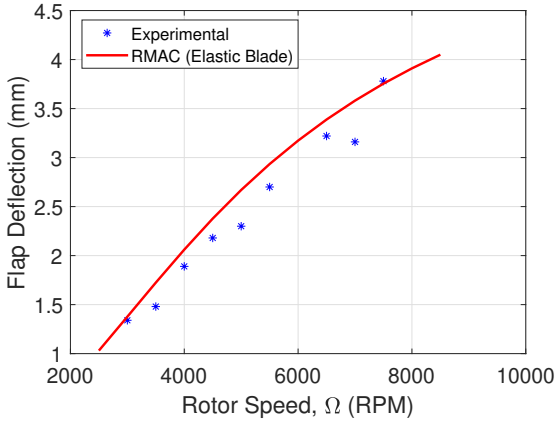

Figure 3: Predicted and experimental flapwise tip deflection – DJI rotor

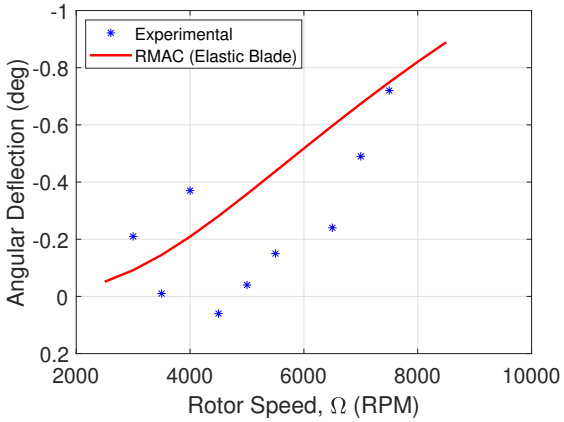

Figure 4: Predicted and experimental torsional tip deflection – DJI rotor

Figure 5: Straight-Up Imaging (SUI) Endurance

The multicopters in this study are derived from the Straight-Up Imaging (SUI) Endurance quadcopter (Fig. 5). To emphasize the influence of rotor elasticity, the stiff carbon-fiber rotors that are normally used on the Endurance are replaced by ABS rotors with the same geometry. Additionally, to examine the effectiveness of rotor phasing on vibration reduction, the rotor speed is locked at 380 rad/s (resulting in a hover tip Mach number of 0.2), and the vehicle is controlled via variable-collective pitch on each rotor. Table 2 lists several parameters of the quadcopter, and the rotor chord and twist are given in Fig. 6.

Table 2: Summary of quadcopter parameters

Quadcopter Parameters	
Rotor Radius	7.5 in (0.1905 m)
Boom Length	12 in (0.3048 m)
Rotor Speed	3626 RPM (380 rad/s)
GTOW	7.04 lb (3.2 kg)

RMAC determines a trim condition for the Endurance derivatives at a given flight speed using the pitch and roll attitudes, as well as the four primary multi-rotor control inputs (Ref. 34). The collective pitch of any rotor is given by Eq.1, where θ_0 is the mean rotor collective pitch (which regulates thrust), θ_{1s} and θ_{1c} are lateral and longitudinal control inputs, and θ_d is the directional input. The θ_{1s} and θ_{1c} control modes are defined using the azimuthal location of the rotor, Ψ_k (see Fig. 7).

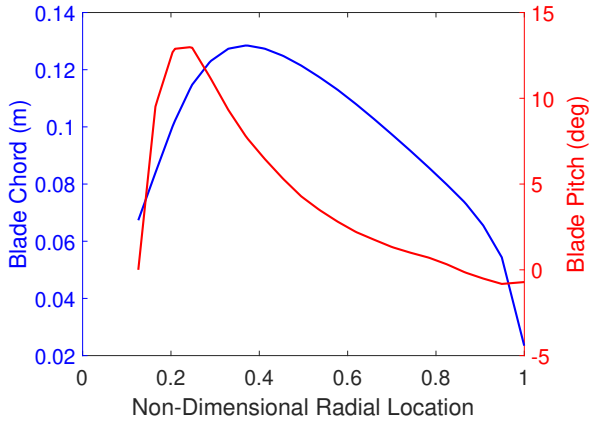

Figure 6: SUI rotor chord and twist distributions

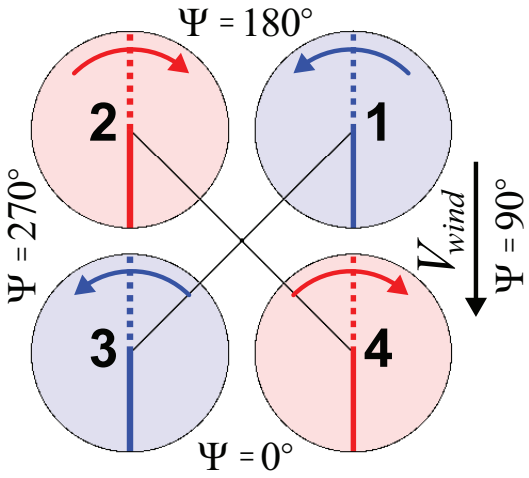

Figure 7: Quadcopter in edge-first configuration with zero relative phasing between rotors

$$\theta_k = \theta_0 + \theta_{1s}\sin\Psi_k + \theta_{1c}\cos\Psi_k + \theta_d(-1)^{k-1} \qquad (1)$$

Individual phase modes are defined for the quadcopter using the same multi-rotor coordinate system as the collective pitch control. The phase of any individual rotor with respect to the phasing shown in Fig. 7 can be described in terms of a pitch (Φ_P), roll (Φ_R), and differential (Φ_D) phasing as shown in Eq. 2. The three phase modes of the quadcopter are illustrated in Fig. 8.

$$\psi_k = \mathrm{sgn}(\cos\Psi_k)\Phi_P + \mathrm{sgn}(\sin\Psi_k)\Phi_R + (-1)^{k-1}\Phi_D + \sum_{i=2}^{\frac{N_r-2}{2}}\left(\mathrm{sgn}(\sin i\Psi_k)\Phi_{is} + \mathrm{sgn}(\cos i\Psi_k)\Phi_{ic}\right) + \Omega t \qquad (2)$$

As Φ_P (Fig. 8a) changes, both of the front rotors lag the reference configuration (Fig. 7) by Φ_P, while the rear two rotors lead the reference configuration by the same amount. Evaluating Eq. 2 for an arbitrary value of Φ_P (other modes held to zero), $\psi_1 = \psi_2$ because $\cos\Phi_1,\ \cos\Phi_2 < 0$. In the context of this study, these rotors will be referred to as "in-phase." Similar to the two front rotors, the two rear rotors are in-phase for all Φ_P ($\psi_3 = \psi_4$). As the rotors turn, rotors 1 and 2 will always

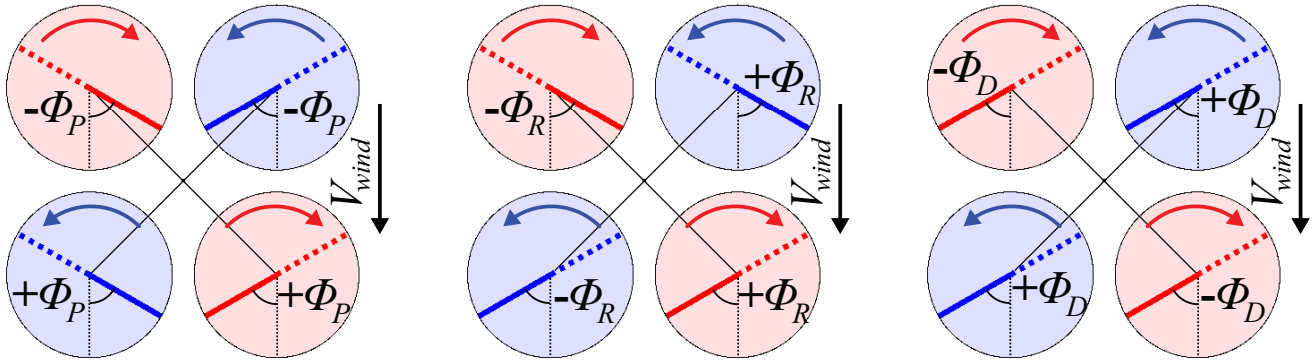

(a) Pitch Phasing, Φ_P (b) Roll Phasing, Φ_R (c) Differential Phasing, Φ_D

Figure 8: Phasing Modes of an edge-first quadcopter

pass one another tip-to-tip, as will rotors 3 and 4. The phase difference between the front and rear rotors is always $2\Phi_P$. It is worth noting, for a $\Phi_P = 0°$ or $90°$, the blades of the front rotor pass tip-to-tip, at the same time the blades of the aft rotors pass tip-to-tip, and the blades of the front rotors also pass the blades of the aft rotor tip-to-tip, but with a quarter revolution phase delay. In contrast, for $\Phi_P = 45°$, the tip-to-top blade passage is phase lagged by a quarter revolution from the tip-to-tip blade passage of the aft rotors. Further, the blades of the front rotor never pass the blades of the aft rotors tip-to-tip (in fact, they have maximum separation).

Φ_R (Fig. 8b) operates in a similar manner but groups the rotors laterally. The blades of the left rotors (2 and 3) will always pass tip-to-tip, thus they remain in-phase for all Φ_R. Since the right rotors (1 and 4) will also remain in-phase, Φ_R effectively modulates a phase difference between the left and right rotor pairs.

Differential phasing Φ_D (Fig. 8c) groups the rotor pairs alternately (rotors 1+3 are paired, as are 2+4). As adjacent rotors also spin in alternate directions, this results in a clockwise (CW) rotor pair, and a counter-clockwise (CCW) rotor pair. As Φ_D changes, $\psi_1 = \psi_3 = \psi_2 + 2\Phi_D = \psi_4 + 2\Phi_D$.

An edge-first octocopter (Fig. 9) of equal disc loading and gross weight is also considered in this study (properties are summarized in Table 3). Like the quadcopter, this vehicle is trimmed using collective pitch control on each individual rotor, with control modes as in Eq. 1. In addition to the three phase modes defined on the quadcopter, four additional modes associated with higher harmonics of Ψ can be defined, and are included in Eq. 2.

In addition to examining the vibratory forces and moments

Table 3: Summary of octocopter parameters

Octcopter Parameters	
Rotor Radius	5.3 in (0.1347 m)
Boom Length	15.7 in (0.3983 m)
Rotor Speed	5128 RPM (537 rad/s)
GTOW	7.04 lb (3.2 kg)

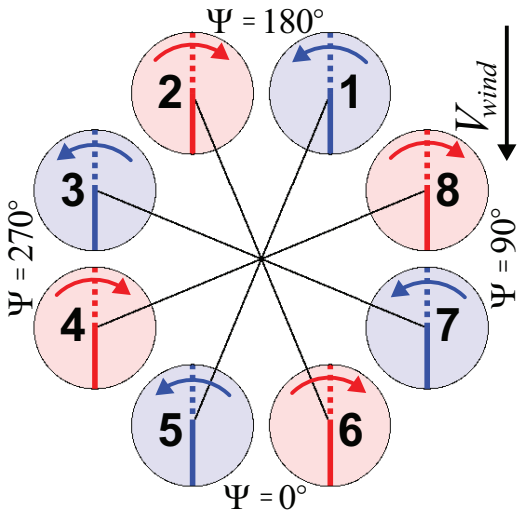

Figure 9: Octocopter in edge-first configuration with zero relative phasing between rotors

along each axis, it is also useful to consider integrated 2/rev force and moment vibration indices. A force and moment vibration index based on a 2-norm is used in this study as defined below.

$$F_{2P} = \sqrt{F_{x,2s}^2 + F_{x,2c}^2 + F_{y,2s}^2 + F_{y,2c}^2 + F_{z,2s}^2 + F_{z,2c}^2}$$
$$M_{2P} = \sqrt{M_{x,2s}^2 + M_{x,2c}^2 + M_{y,2s}^2 + M_{y,2c}^2 + M_{z,2s}^2 + M_{z,2c}^2} \quad (3)$$

RESULTS

Isolated Rotor

In forward flight, the quadcopter will require a differential root pitch between the front and rear rotors (Ref. 28) to counteract the nose-up pitching moment produced by each rotor, in addition to a nose-down attitude required to overcome aircraft drag. At 13 m/s, the vehicle operates at 16.2° nose-down pitch attitude and the front rotors operate at 9.3° root pitch. The aerodynamic lift on the blade is plotted in Fig. 10. Due

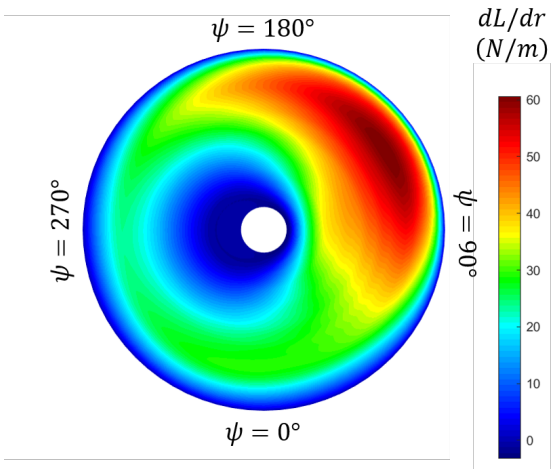

Figure 10: Lift distribution of front-right rotor trimmed at 13 m/s

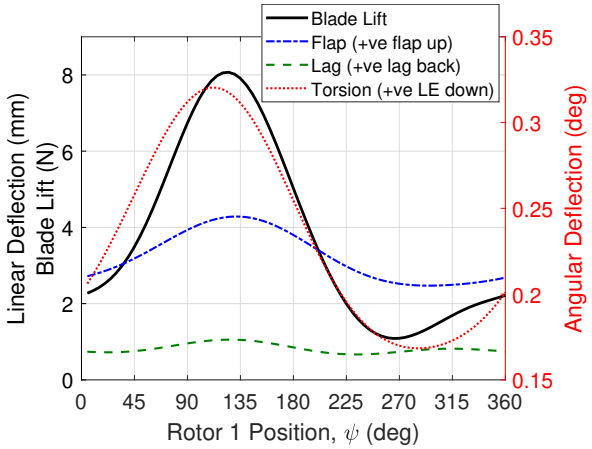

Figure 11: Isolated rotor deflections

to the dynamic pressure variation, the lift is biased toward the advancing side of the disk, and due to the longitudinal inflow distribution, it is also biased toward the front of the disk.

The aerodynamic lift is the dominant contributor to the flapwise deflection of the rotor blade, shown in Fig. 11. The flapwise deflection of the blade lags the blade lift by 15° ($\nu_\beta = 1.28$) due to the stiffness of the blades. Due to the highly twisted blade, the lift does not act along the principal axes of the airfoil section, so the lag (in-plane) deflection is also dominated by the lift, and is in-phase with the flapwise deflection. The torsional deflection is also in-phase with the lift.

The flapwise deflection of the blades causes inertial vertical shears at the root of the blade, which are generally in-phase with the aerodynamic loads (Fig. 12); lead/lag motion will additionally produce a root shear. The vertical motion of the blades will also produce a flapwise root bending moment. Aerodynamic pitching moment and torsional acceleration will produce blade root torsional moments, though these moments are small compared to the flapwise moments. Summing the blade root shears and moments over the two blades results in 2/rev-dominant vibratory hub forces and moments.

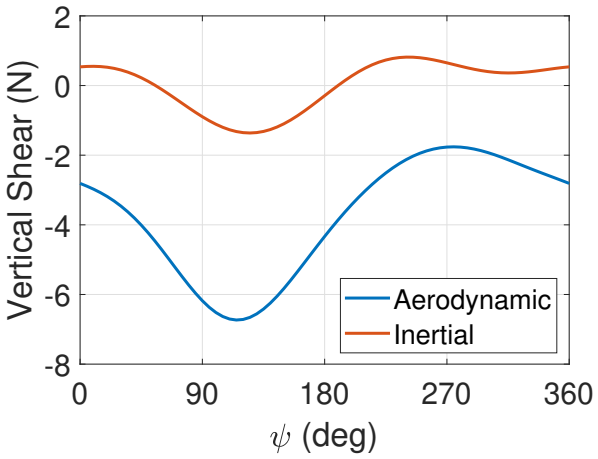

Figure 12: Blade root vertical shear for front right rotor trimmed at 13 m/s (Note: positive is defined as downward)

This process can be repeated for the other rotors in the system. Rotor 2, for example, operates at an identical root pitch and nose-down attitude, but rotates in the opposite direction from rotor 1. Thus, it will have a lift distribution similar to Fig. 10, except reflected about the 0°-180° line. Thus, the 2/rev side force and roll moment, will have identical magnitude, but opposite sign, and the drag, thrust, and pitching moment have equal magnitude and sign. For the phasing illustrated in Fig. 7, the forces and hub moments are plotted in Fig. 13. The magnitude of the 2/rev forces and moments for the front rotors' is also given in Fig. 14

Quadcopter

Pitch Phasing As Φ_P is varied, the two front rotors will always remain in-phase with each other, as will the two rear rotors. Each rotor within these pairs operates at identical root pitch, but have opposite spin directions. Thus, the side force, as well as the hub rolling moment, will cancel, and the thrust, drag, and hub pitching moments will compound. As the lateral forces and hub moments within each rotor pair cancel, these will not contribute to net 2/rev vibration at the aircraft level for any Φ_P. Further, because the rotor thrust in each rotor pair is in-phase, and these rotors are on opposite sides of the rolling axis, the 2/rev rolling moment these rotors induce will also cancel. However, the pitching moment induced by thrust will compound.

The magnitude of the 2/rev net forces and moments about each axis of the quadcopter as Φ_P is varied from 0° to 90° (with all other modes held to zero) is plotted in Fig. 15. When $\Phi_P = 0°$, all four rotors are in-phase with one another. Consequently, the 2/rev rotor drag and thrust are in-phase.

As Φ_P increases from 0°, the front rotor pairs become increasingly out-of-phase with the rear rotors. Thus, as shown in Fig. 16, the thrust produced by these pairs of rotors are increasingly out-of-phase. Consequently, the net 2/rev thrust on the aircraft decreases. At $\Phi_P = 45°$, the phase between the front and rear rotors is exactly 90°. In this case, the front rotors (which still pass each other tip-to-tip), will pass the

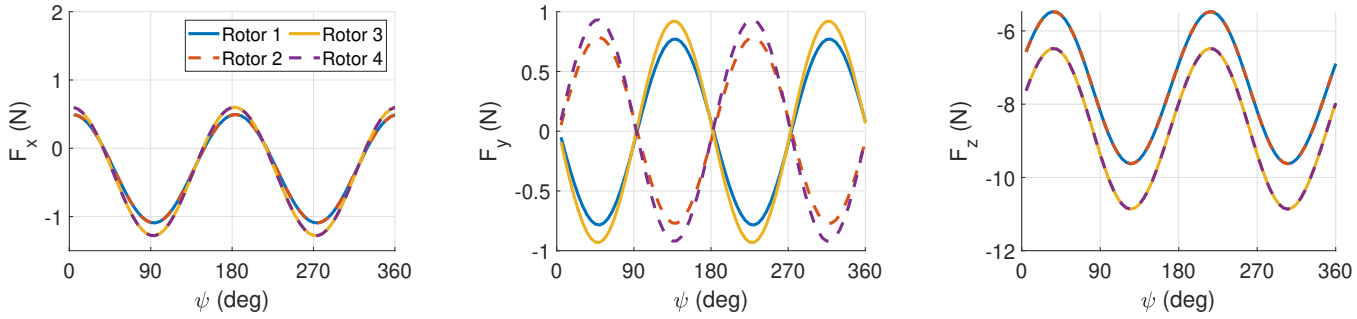

(a) Drag Force (b) Side Force (c) Vertical Force

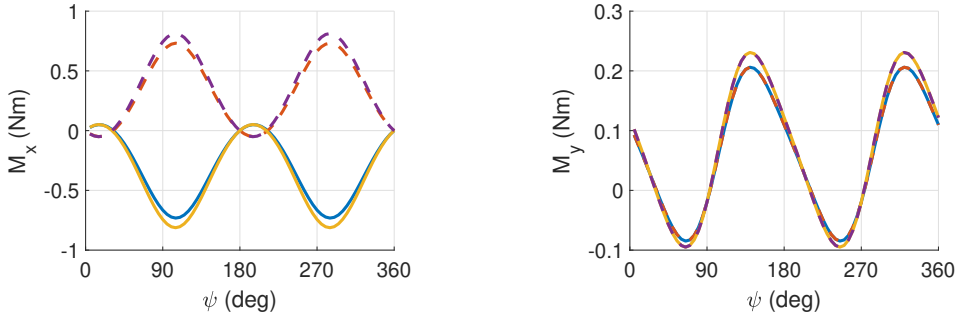

(d) Hub Roll Moment (e) Hub Pitch Moment

Figure 13: Rotor Hub Loads at 13 m/s trimmed flight

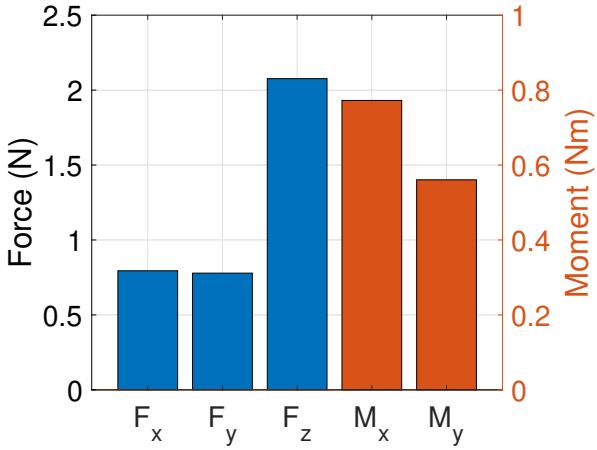

Figure 14: 2/Rev Amplitude of Hub Forces and Moments for Front Rotor Trimmed at 13 m/s

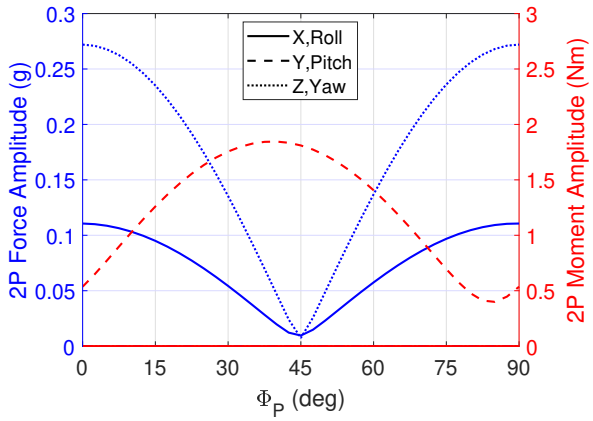

Figure 15: Quadcopter amplitude of 2/rev vibratory forces and moments at aircraft C.G. using pitch phasing (V = 13m/s)

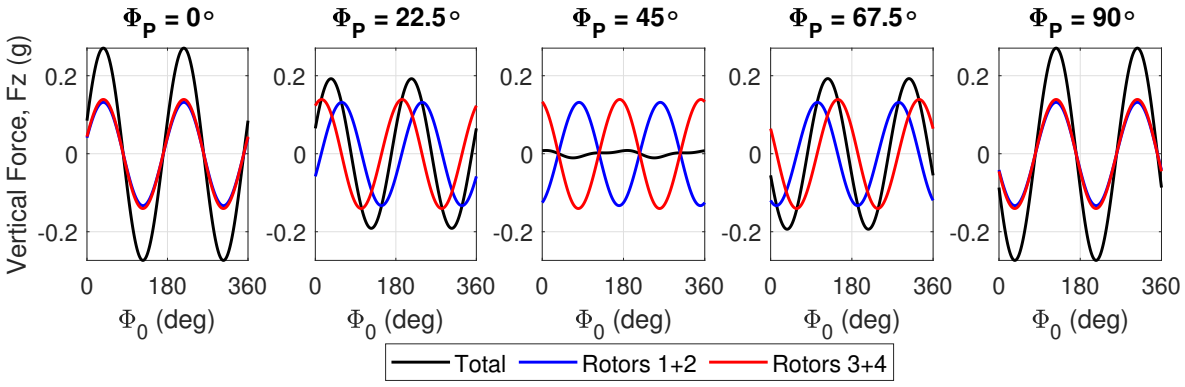

Figure 16: Quadcopter 2/rev vertical forces at aircraft C.G. using pitch phasing (V = 13m/s)

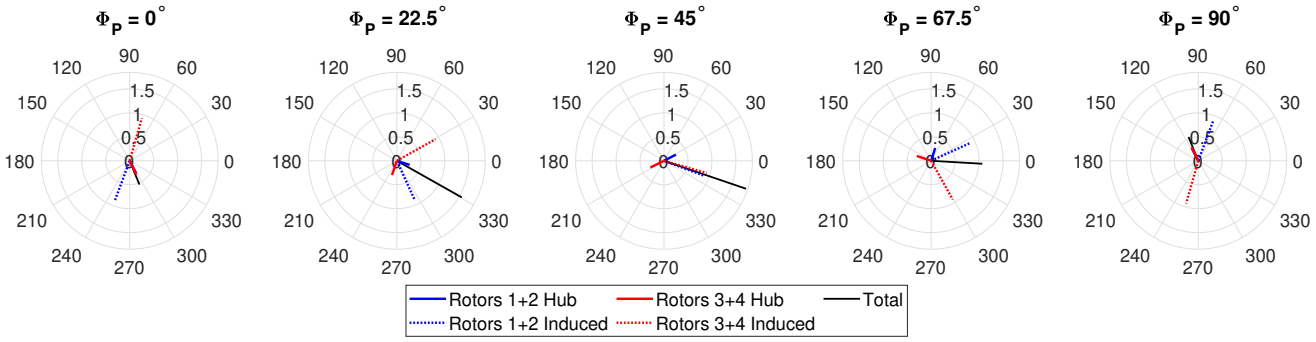

Figure 17: Quadcopter amplitude and phase of net 2/rev hub and force induced pitching moments at aircraft C.G. using pitch phasing (V = 13m/s)

rear rotors orthogonally (i.e., when the front rotors' blades are alinged forward-backward, the rear rotors' blades are aligned left-right), and the 2/rev forces are completely out-of-phase. The same argument holds for the 2/rev drag, which follows the same trend as thrust in Fig. 15. Thus, there is a minimum in force vibration on all axes at $\Phi_P = 45°$, though the cancellation is not perfect, as the rear rotors are more heavily loaded than the front rotors in forward flight. Relative to the baseline case ($\Phi_P = 0°$), the 2/rev thrust and drag are reduced by 97.3% and 93.3%, respectively.

The net 2/rev moments about the vehicle C.G. are also plotted versus Φ_P in Fig. 15. The pitch moment behaves much differently than thrust and drag, because the vehicle moment about any axis has two sources, namely the moments about each rotor's hub, which are transmitted directly from the hub of each rotor to the vehicle, and force-induced moments (as each rotor has a moment arm). For no value of Φ_P do the pitching moments cancel entirely. This is due to the interaction between the hub and thrust-induced moments, illustrated in Fig. 17. When $\Phi_P = 0°$, the thrusts of the front/rear rotor are in-phase, so the induced moments of the front and rear rotors are out-of-phase. However, at the same time, the hub moments are in-phase. Conversely, at $\Phi_P = 45°$, the hub pitching moment is out-of-phase, while the thrust-induced moments are in-phase.

Roll Phasing Similar to how the use of Φ_P left the front (and rear) two rotors in phase with one another, the use of Φ_R will keep the two right (and two left) rotors in-phase. Like Φ_P, each rotor pair contains one CW rotor, and one CCW rotor. As a result, the side forces and hub rolling moments will mostly cancel, but not entirely, since the two rotors are operating at different pitch settings. The drag, thrust, and hub pitching moments will again compound within the rotor pair.

Consequently, the behavior of the 2/rev drag and vertical forces on the vehicle are very similar, as shown in Fig. 18. However, the imbalance in the rotor side forces within each pair results in a small net 2/rev side force within each rotor pair, resulting in a small net 2/rev side force for $\Phi_R \neq 0$. Overall, the 2/rev forces can be reduced by 96.7%.

As the two rotors within each pair are on opposite sides of the pitching axis, the net 2/rev induced pitching moment is

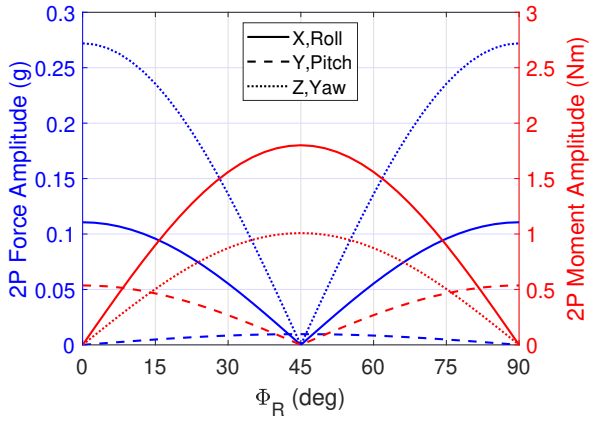

Figure 18: Quadcopter amplitude of 2/rev vibratory forces and moments at aircraft C.G. using roll phasing (V = 13m/s)

very small for all Φ_R. As a result, the pitching moment can be entirely cancelled at $\Phi_R = 45°$, where the phase between the left and right rotors is 90° (when the left rotors' blades are aligned forward-backward, the right rotors' blades are aligned left-right). However, this results in a very large 2/rev thrust-induced rolling moment, similar to the induced pitching moment at $\Phi_P = 45°$. It is also accompanied by a large yawing moment, due to the 2/rev moment induced by the rotors' in-plane forces (both drag and side force).

Differential Phasing Φ_D results in pairing of rotors by their spin direction. Counter-clockwise (CCW) spinning (and clockwise-spinning) rotors will always remain in phase with one another. Unlike Φ_P and Φ_R, there is no cancellation of forces or hub moments within a rotor pair. However, as the rotors within each pair are on opposite sides of the center of gravity, all force-induced moments cancel within each pair.

Similar to Φ_P and Φ_R, 45° of Φ_D results in a minimization of the 2/rev vertical and longitudinal forces (Fig. 19), as the CCW rotors' thrust and drag are out-of-phase with those of the CW rotors. Unlike pitch and roll phasing, side forces compound, rather than cancel, within each rotor pair, resulting in a large 2/rev lateral force when $\Phi_D = 45°$ (when the CCW and CW rotors are 90° out-of-phase). Relative to the baseline

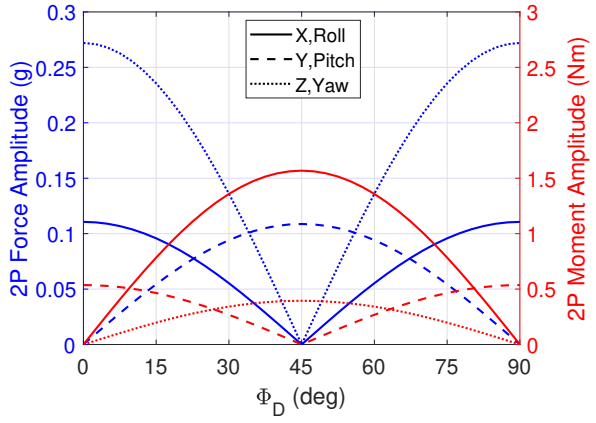

Figure 19: Quadcopter amplitude of 2/rev vibratory forces and moments at aircraft C.G. using differential phasing (V=13m/s)

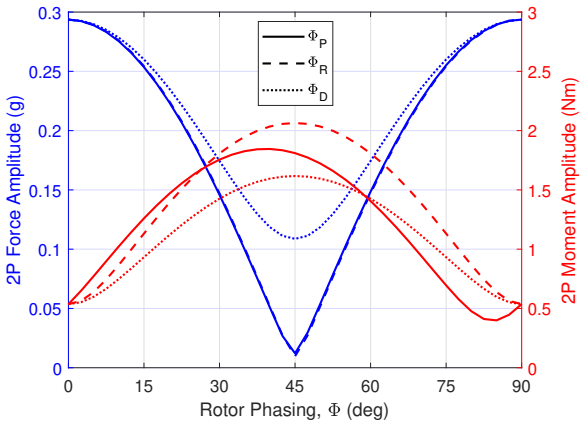

Figure 20: Quadcopter 2-norm force and moment amplitudes for individual phase modes

case, the overall force vibration can only be reduced by 63%, rather than the over 90% reduction using Φ_P and Φ_R.

Because the the force-induced moments of each rotor pair largely cancel for all Φ_D, only the rotor hub moments can contribute to the net moments acting on the vehicle. For $\Phi_D = 0°$, the hub rolling and yawing moments of the CCW and CW rotors are out-of-phase, while at $\Phi_D = 45°$, these moments compound. The opposite occurs for pitching moment, which behaves precisely like it did with Φ_R.

Using the 2-norm force and moment vibration indices from Eq. 3, Fig. 20 shows the overall 2/rev force and moment vibration using each of the three phasing modes. Φ_P and Φ_R show similar of 2/rev forces, and much greater reduction than Φ_D. From Fig. 20, it would appear that $\Phi_P = 45°$ results in the lowest overall vibration, with 2/rev forces nearly eliminated, and lower vibratory moment than either Φ_R or Φ_D, though none of the individual modes is capable of simultaneously reducing 2/rev forces and moments.

Octocopter

The octocopter has a total of seven phase modes. In addition to the three pitch, roll, and differential modes previously described for the quadcopter, one mode is associated with $\sin 2\Psi$, $\cos 2\Psi$, $\sin 3\Psi$, and $\cos 3\Psi$. For brevity, only a subset of these modes (Φ_P, Φ_{2s}, and Φ_{2c}, Fig. 21) will be presented, as these were most effective for aircraft-level vibration reduction.

Pitch Phasing As with the quadcopter, Φ_P on the octocopter (Fig. 21a) enforces a phase difference between the front rotors (1, 2, 3, and 8 in Fig. 9) and rear rotors (4–7). The 2/rev forces and moments at the C.G. of the octocopter are plotted versus Φ_P in Fig. 22. Qualitatively, the behavior of each force and moment is similar to the quadcopter, with both 2/rev thrust and drag being cancelled at the aircraft level for $\Phi_P = 45°$ (when the front/rear rotors are 90° out of phase). Similarly, the interaction between the thrust-induced and hub pitching moments prevents complete cancellation, as the point

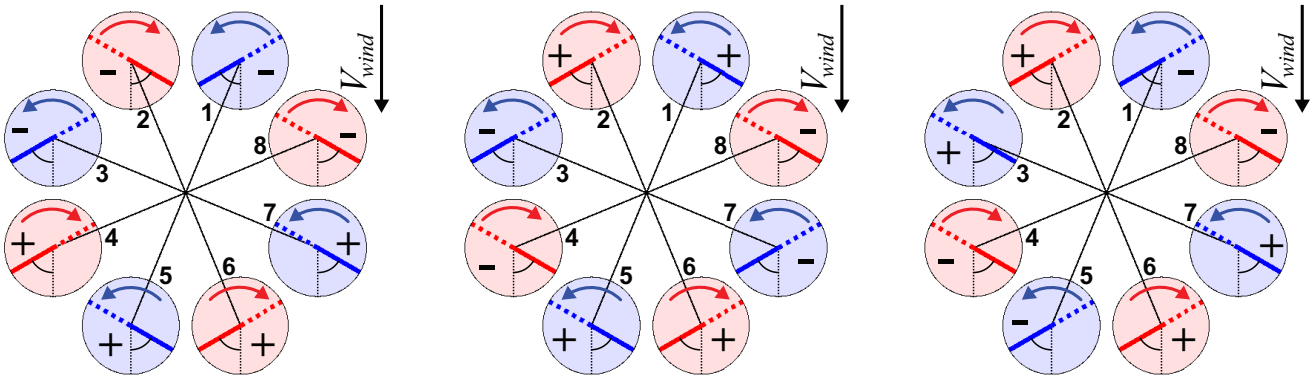

(a) Pitch Phasing, Φ_P (b) 2c Phasing, Φ_{2c} (c) 2s Phasing, Φ_{2s}

Figure 21: Phasing Modes of an edge-first octocopter

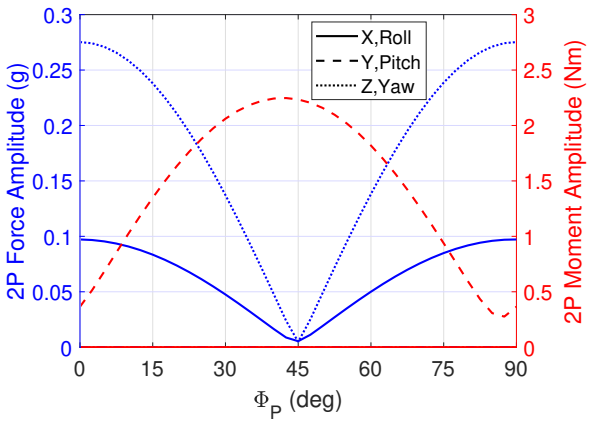

Figure 22: Octocopter amplitude of 2/rev vibratory forces and moments at aircraft C.G. using pitch phasing (V=13m/s)

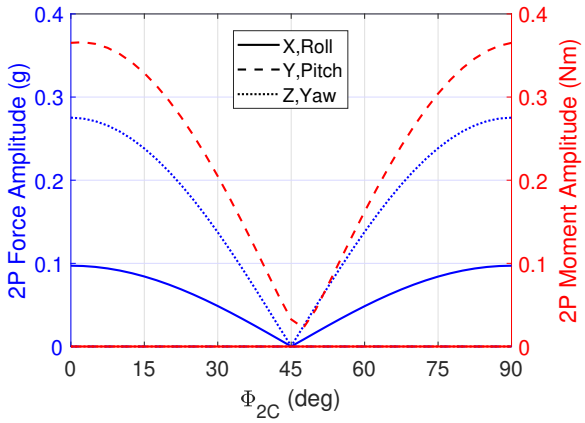

Figure 23: Octocopter amplitude of 2/rev vibratory forces and moments at aircraft C.G. using 2c phasing (V=13m/s)

where hub moments are minimized ($\Phi_P = 45°$), the thrust-induced moments are maximized, and vice-versa. All lateral forces/moments cancel within rotor pairs (rotors 1+2 cancel, as do rotors 3+8, 4+7, 5+6) for all Φ_P, just as they did with the quadcopter. The similarities between the octocopter and quadcopter extend to Φ_R and Φ_D, as the similar definitions of the phase modes produces similar behavior of the vibratory forces and moments.

2c Phasing Φ_{2c} generates a relative phase between the longitudinally extreme rotors (1, 2, 5, and 6), and the laterally extreme rotors (3, 4, 7, and 8) as shown in Fig. 21b. The 2/rev forces and moments are plotted versus Φ_{2c} in Fig. 23. As was the case with Φ_P, the side force cancels within rotor pairs (1+2, 3+8, 4+7, and 5+6), since these rotors are always in-phase and spin in opposite directions. Similarly, both the hub and force-induced rolling moments and yawing moments cancel within these same rotor pairs. Thrust and drag also behave similarly to the other phase modes, with a minimum at $\Phi_{2c} = 45°$, where the longitudinally extreme rotors are out-of-phase with the laterally extreme rotors.

The only major difference between Φ_{2c} on the octocopter and the other phase modes examined thus far is in the pitching moment, which is broken down into its hub and force-induced

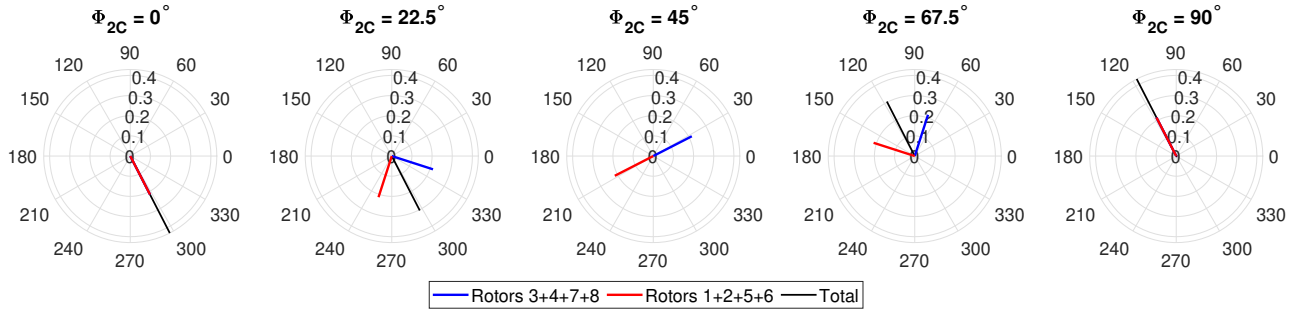

(a) Hub moment

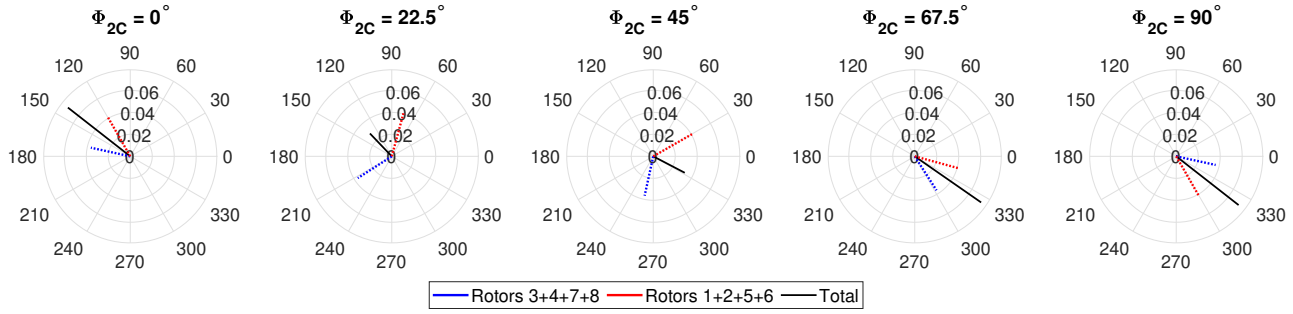

(b) Force-induced moment

Figure 24: Hub and force-induced pitching moments on an octocopter V = 13m/s at various Φ_{2c}

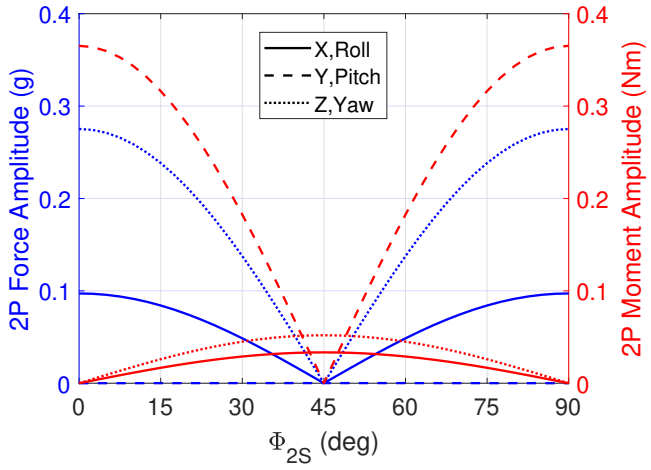

Figure 25: Octocopter amplitude of 2/rev vibratory forces and moments at aircraft C.G. using 2s phasing (V=13m/s)

components in Fig. 24. Because diametrically opposed rotors (1+5, 2+6, 3+7, and 4+8) are always in-phase, the thrust produced within these pairs are also in-phase. Since these rotors are also on opposite sides of the C.G., the pitching moment induced by these rotors mostly cancels for all Φ_{2c} (compare the radial scale on Fig. 24b to that on Figs. 24a). Thus, the total pitching moment is dominated by the hub moment, which will mostly cancel at $\Phi_{2c} = 45°$. Thus, unlike the quadcopter, the octocopter is capable of simultaneously reducing both the forces and the moments substantially using rotor phasing. With maximum reductions of 99.8% and 91.1% for the vibratory forces and moments respectively, relative to the baseline phasing.

2s Phasing Φ_{2s} (Fig. 21c) creates a phase difference between the northwest/southeast rotors and the northeast/southwest rotors. The 2/rev forces and moments experienced by the octocopter as Φ_{2s} is varied (Fig. 25) is somewhat similar to Φ_{2c}, though there are some differences. In particular, the pitching moment completely cancels at $\Phi_{2s} = 45°$, while there is a local maximum (still very low) in the rolling and yawing moment. The complete cancellation can occur because at $\Phi_{2s} = 45°$, both the thrust and hub pitching moments between rotors 1 and 2 (and 3+8, 4+7, and 5+6) are out-of-phase. Since these rotors are on the same side of the pitching axis, their thrust-induced pitching moments will cancel. Between the four pairs of rotors, the aircraft level rolling and yawing moments mostly cancel, as well. Overall, the vibratory moments are reduced by 83.1% for $\Phi_{2s} = 45°$.

These three phase modes are compared using the 2-norm force and moment vibration indices in Fig. 26. All three modes are equally capable of reducing the overall 2/rev vibratory forces, but Φ_{2c} and Φ_{2s} are strictly superior to Φ_P in 2/rev vibratory moments, and can simultaneously reduce all forces and moments to near-zero levels, showcasing the octocopter's superior potential for aircraft-level vibration reduction using relative rotor phasing as compared to the quadcopter, which does not have higher harmonic phase modes.

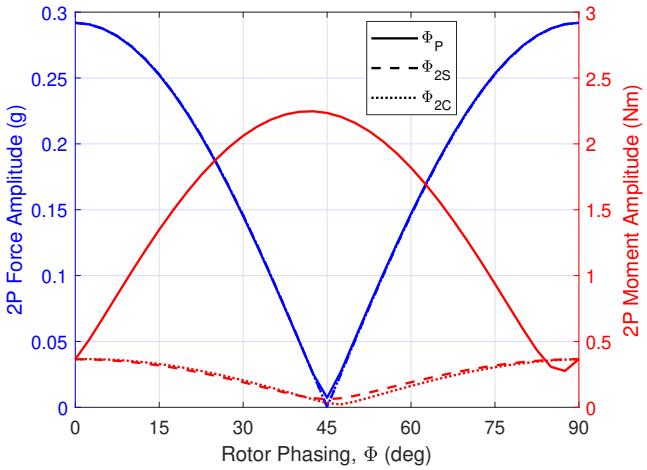

Figure 26: Octocopter 2-norm force and moment amplitudes for individual phase modes

Multiple Phase Modes

Varying only individual phase modes reveals only a small portion of the available design space. To understand the interaction of multiple phase modes used simultaneously, and to identify whether any additional vibration reduction is possible, the design space is explored systematically. A uniform grid of points is constructed, each of which represents a single set of rotor phases. For each point, the 2-norm force and moment vibration indices are evaluated. From this data, a set of Pareto-optimal rotor phases can be constructed, from which a designer can select based on relative importance of force and moment vibration reduction.

Fig. 27 shows the space of vibratory force and moment reachable using rotor phasing on the quadcopter. Included in the figure are curves corresponding to single phase mode variations. It can be seen that Φ_P strictly dominates both Φ_R and Φ_D, with the lower branch having both lower vibratory force and moment. In fact, the Φ_P curve coincides with the Pareto front in multiple places, including the minimizer associated with equal force and moment weighting (represented by the green cross). However, there is a substantial region of the Pareto front that is not reachable using any single phase mode.

If it were critically important to reduce the 2/rev moment,

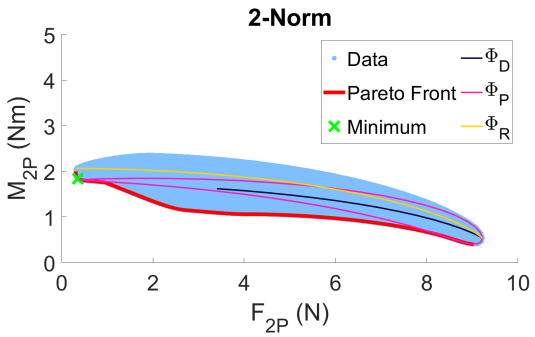

Figure 27: Force and moment vibration on a quadcopter

even at the expense of increased 2/rev forces, one could weight moment more heavily than force in the evaluation of a composite vibration index (Eq. 4), where $W = 0$ disregards moment entirely, and $W = 1$ uses moment exclusively. The optimal rotor phasing using a single mode and multiple modes are listed in Table 4.

Table 4: Use of Single- and Multiple Phase Modes for Minimization of the Quadcopter's Composite Vibration Index

	W	Mode	Value	F_{2P} (N)	M_{2P} (Nm)	Vibration Index
Single Phase	0.5	Φ_R	0	0.38	1.81	1.10
		Φ_P	45°			
		Φ_D	0			
	0.8	Φ_R	0	0.38	1.81	1.52
		Φ_P	45°			
		Φ_D	0			
Multiple Phase	0.5	Φ_R	0	0.38	1.81	1.10
		Φ_P	45°			
		Φ_D	0			
	0.8	Φ_R	0	1.74	0.84	1.01
		Φ_P	21.5°			
		Φ_D	45°			

For $W = 0.5$, the individual mode (Φ_P) reaches the overall minimum at 45° but the system is unable to reduce the moment vibration without very large increases in the force vibration (the slope of the magenta curve in Fig. 27 is very small). For $W = 0.8$ (4:1 moment-force weighting), however, using Φ_D in conjunction with Φ_P allows moment to be reduced by 54% while increasing the (lightly weighted) force vibration, for an overall vibration index reduction of 33%.

$$\text{Composite Vibration Index} = (1-W)F_{2P} + WM_{2P} \quad (4)$$

A similar exercise was conducted on the octocopter, and the space of vibratory force and moment is given in Fig. 28. As was seen in the single phase mode results, force and moment can be minimized simultaneously by either Φ_{2s} or Φ_{2c}, though none of the other phase modes can achieve this.

Absent a phase control system, the rotors would be randomly phased relative to one another (even with RPM synchronization), with a net 2/rev force and moment falling somewhere in

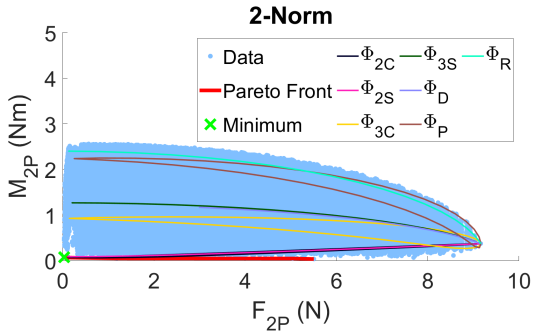

Figure 28: Force and Moment vibration on an octocopter

Table 5: Comparison of vibration-optimized phasing for $W = 0.5$

Case	Vibration Index	
	Quadcopter	Octocopter
Optimal	1.10	0.054
Mean	3.08	2.22
Worst-Case	4.92	4.85

the blue space of Figs. 27 or 28. Table 5 compares the vibration levels for the $W = 0.5$ (equal force/moment weighting) vibration index minimizers (green crosses in Figs. 27 and 28) to the mean of all the possible phase combinations (reasonably representative of a random phasing) and the worst-case phasing.

On average, the octocopter has overall lower vibration than the quadcopter, due to the presence of more rotors, increasing the likelihood that some rotors are out-of-phase with the others, though the worst-case scenarios are very similar between the two aircraft. Both vehicles experience their worst-case 2/rev vibration when all of the rotors are in-phase, or nearly in-phase. Compared to the mean vibration levels, the phase-optimized quadcopter has 62% reduced overall vibration, and the octocopter has 96% reduced overall vibration.

CONCLUSIONS

The relative phasing of synchronized fixed-RPM, variable-pitch rotors on a quadcopter and an octocopter was explored for vibration reduction. Several phase modes were defined for each aircraft with the multi-rotor coordinate transform, including a pitch mode which represents a phase difference between the front rotors and rear rotors, a roll mode which represents a phase difference between the left and right rotors, and a differential mode which represents the phase difference between CW and CCW rotors. Additional higher harmonic modes were defined on the octocopter.

From the single-mode analysis of the quadcopter, both pitch and roll phasing allowed for the greatest reduction in vibratory forces with a maximum reductions of 95.9% and 96.7% respectively from the baseline phase when Φ_R or $\Phi_P = 45°$. Although minimized at the same point ($\Phi_D = 45°$), the differential phasing was less effective at reducing vibratory forces with only a reduction of 63.0% due to the introduction of significant 2/rev side forces not seen with Φ_R and Φ_P.

However, this reduction of vibratory forces comes at the cost of an increase in vibratory moments. For both Φ_R and Φ_D, the vibratory moments are lowest when all rotors are in-phase ($\Phi = 0°$), and greatest at $\Phi_R = 45°$ or $\Phi_D = 45°$. For Φ_P, pitch moment was never reduced to zero due to the interaction between thrust-induced moment and hub pitching moment.

The octocopter has additional four phasing modes which allow the vibratory forces and moments to be reduced simultaneously. Both Φ_{2s} and Φ_{2c} reduce the vibratory forces by 99.8% at 45°. At the same time, these modes reduce the vibratory moment about the C.G. by 83.1% and 91.1% respectively.

Simultaneously varying multiple phase modes created a comprehensive set of possible force and moment vibration levels, from which a Pareto front was constructed. On the quadcopter, Φ_P formed part of this Pareto front, though could not reach a Pareto-optimal solution for some moderate force-to-moment weighting. In this region, the use of multiple phase modes can reduce the overall vibration level by 33% (for a 4:1 moment-to-force weighting).

The search also allowed a comparison of the optimal solutions to the mean and worst-case vibration levels. Compared to vibration levels in forward flight that might, on average, be expected if the rotors were randomly phased, reductions of 62% and96% in a composite vibration index (equally weighting 2/rev vibratory forces and moments) were calculated for the quadcopter and octocopter, respectively, with appropriate rotor phasing.

ACKNOWLEDGEMENTS

This work is carried out at Rensselaer Polytechnic Institute under the Army/Navy/NASA Vertical Lift Research Center of Excellence (VLRCOE) Program, grant number W911W61120012, with Dr. Mahendra Bhagwat as Technical Monitor.

REFERENCES

1. Holden, J., and Goel, N., "Fast-Forwarding to a Future of On-Demand Urban Air Transportation," Uber Elevate Whitepaper, October 2016, Available at: https://www.uber.com/elevate.pdf [Accessed 10 Oct. 2019].

2. NASA, "NASA's UAM Grand Challenge," , August 2019, Available at: https://www.nasa.gov/uamgc [Accessed 10 Oct. 2019].

3. Swartz, K., "NASA Embraces Urban Air Mobility," Vertiflite Magazine, Jan-Feb 2019.

4. Johnson, W., Silva, C., and Solis, E., "Concept Vehicles for VTOL Air Taxi Operations," AHS International Technical Meeting on Aeromechanics Design for Transformative Vertical Flight, San Francisco, CA, January 16–18, 2018.

5. Yoon, S., Lee, H., and Pulliam, T., "Computational Analysis of Multi-Rotor Flows," AIAA 54th Aerospace Sciences Meeting, San Diego, CA, January 2016.

6. seokkwan Yoon, Diaz, P. V., Boyd, D. D., , Chan, W., and Theodore, C., "Computational Aerodynamic Modeling of Small Quadcopter Vehicles," 73rd VFS Annual Forum, Fort Worth, TX, May 9–11, 2017.

7. Diaz, P. V., and Yoon, S., "High-Fidelity Computational Aerodynamics of Multi-Rotor Unmanned Aerial Vehicles," AIAA SciTech Forum 2018, Kissimmee, Florida, January 8–12, 2018.

8. Misiorowski, M., Gandhi, F., and Oberai, A., "Computational Study on Rotor Interactional Effects for a Quadcopter in Edgewise Flight," *AIAA Journal*, Vol. 57, (12), December 2019. DOI: 10.2514/1.J058369

9. Healy, R., Misiorowski, M., and Gandhi, F., "A Systematic CFD-Based Examination of Rotor-Rotor Separation Effects on Interactional Aerodynamics for LArge eVTOL Aircraft," 75th VFS Annual Forum, Philadelphia, PA, May 13–16, 2019.

10. Healy, R., Gandhi, F., Mistry, M., and Duffy, M., "A Computational Investigation of Multi-Rotor Interactional Aerodynamics with Hub Lateral and Longitudinal Canting," VFS 76th Annual Forum, October 6–8, 2020.

11. Intaratep, N., Alexander, W., Devenport, W., Grace, S., and Dropkin, A., "Experimental Study of Quadcopter Acoustics and Performance at Static Thrust Conditions," 22ns AIAA/CEAS Aeroacoustics Conference, Lyon, France, May 2016.

12. Tinney, C., and Sirohi, J., "Multirotor Drone Noise at Static Thrust," *AIAA Journal*, Vol. 56, (7), 2018.

13. Passe, B., and Bader, J., "Computational Aeroacoustics of Different Propeller Configurations for eVTOL Applications," VFS Autonomous VTOL Technical Meeting and Electric VTOL Symposium, Mesa, AZ, January 2019.

14. Quackenbush, T., Wachspress, D., Ricci-Moretti, L., Barwey, D., Lewis, R., and Brentner, K., "Aeroacoustic Modeling of an eVTOL Slowed Rotor Winged Compound Aircraft," 75th VFS Annual Forum, Philadelphia, PA, may 13–16, 2019.

15. Jia, Z., and Lee, S., "Acoustic Analysis of Urban Air Mobility Quadrotor Aircraft," Transformative Vertical Flight 2020, San Jose, CA, jan 21–23, 2020.

16. Wachspress, D., Yu, M., and Brentner, K., "Rotor/Airframe Aeroacoustic Prediction for eVTOL UAM Aircraft," 75th VFS Annual Forum, Philadelphia, PA, may 13–16, 2019.

17. Zhang, J., Brentner, K., and Smith, E., "Prediction of the Aerodynamic and Acoustic Impact of Propeller-Wing Interference," Transformative Vertical Flight 2020, San Jose, CA, January 21–23, 2020.

18. Schiller, N., Pascioni, K., and Zawodny, N., "Tonal Noise Control using Rotor Phase Synchronization," 75th VFS Annual Forum, Philadelphia, PA, May 13–16, 2019.

19. Pascioni, K., Rizzi, S., and Schiller, N., "Noise Reduction Potential of Phase Control for Distributed Propulsion Vehicles," AIAA 2019 SciTech Forum, San Diego, CA, January 7–11, 2019.

20. Smith, B., Niemiec, R., and Gandhi, F., "A Comparison of Multicopter Noise Characteristics with Increasing Number of Rotors," 76th VFS Annual Forum, Virginia Beach, VA, October 6–8, 2020.

21. Walter, A., McKay, M., Niemiec, R., Gandhi, F., and Jaran, C., "An Assessment of Heave Response Dynamics for Electrically Driven Rotors of Increasing Diameter," 8th Biennial Autonomous VTOL Technical Meeting, 6th Annual Electric VTOL Symposium, Mesa, AZ, January 29–31, 2019.

22. Walter, A., McKay, M., Niemiec, R., Gandhi, F., and Ivler, C., "Handling Qualities Based Assessment of Scalability for Variable-RPM Electric Multi-Rotor Aircraft," 75th VFS Annual Forum, Philadelphia, PA, May 13–16, 2019.

23. Walter, A., McKay, M., Niemiec, R., Gandhi, F., and Ivler, C., "Hover Handling Qualities of Fixed-Pitch, Variable-RPM Quadcopters with Increasing Rotor Diameter," 76th VFS Annual Forum, Virginia Beach, VA, October 6–8, 2020.

24. Bahr, M., McKay, M., Niemeic, R., and Gandhi, F., "Performance and Handling Qualities Assessment of Large Variable-RPM Control Multi-Rotor Aircraft for Urban Air Mobility," VFS 76th Annual Forum, Virgina Beach, VA, October 6–8, 2020.

25. Malpica, C., and Withrow-Maser, S., "Handling Qualities Analysis of Blade Pitch and Rotor Speed Controlled eVTOL Quadrotor Concepts for Urban Air Mobility," VFS Inernational Powered Lift Conference 2020, San Jose, CA, January 21–23, 2020.

26. Niemiec, R., Gandhi, F., Lopez, M., and Tischler, M., "System Identification and Handling Qualities Perdictions of an eVTOL Urban Air Mobility Aircraft Using Modern Flight Control Methods," 76th VFS Annual Forum, Virginia Beach, VA, October 6–8, 2020.

27. Niemiec, R., and Gandhi, F., "Effect of Elastic Blade Deformation on Trim and Vibratory Loads of a Quadcopter," 73rd VFS Annual Forum, Fort Worth, TX, May 9–11, 2017.

28. McKay, M., Niemiec, R., and Gandhi, F., "Performance Comparison of Quadcopters with Variable-RPM and Variable-Pitch Rotors," *Journal of the American Helicopter Society*, Vol. 64, (4), 2019, pp. 042006–1–042006–14.

29. Kopyt, N., Niemiec, R., and Gandhi, F., "Quadcopter Rotor Phasing for Minimization of Aircraft Vibratory Loads," Transformative Vertical Flight 2020, San Jose, CA, January 21–23, 2020.

30. Niemiec, R., and Gandhi, F., "Development and Validation of the Rensselaer Multicopter Analysis Code (RMAC): A Physics-Based Comprehensive Modeling Tool," 75th Annual VFS Forum, Philadelphia, PA, May 13–16, 2019.

31. Hodges, D., and Dowell, E., "Nonlinear Equations of Motion for the Elastic Bending and Torsion of Twisted Nonuniform Rotor Blades," Technical Note TN D-7818, National Aeronautics and Space Administration, December 1974.

32. Peters, D., Boyd, D., and He, C. J., "Finite-State Induced-Flow Model for Rotors in Hover and Forward Flight," *Journal of the American Helicopter Society*, Vol. 34, (4), 1989, pp. 5–17.

33. Nowicki, N., *Measurement and Modeling of Mulitcopter UAS Rotor Blade Deflection in Hover*, Master's thesis, KTH - Royal Institute of Techonology, July 2016.

34. Niemiec, R., and Gandhi, F., "Multi-Rotor Coordinate Transform for Orthogonal Primary and Redundant Control Modes for Regular Hexacopters and Octocopters," 42nd European Rotorcraft Forum, Lille, France, September 5–8, 2016.